https://doi.org/10.1016/j.yofte.2015.03.004

Investigation of microwave photonic filters based on multi-longitudinal-mode fiber laser source

Yuan Cao,[a] Feng Li,[b] Xinhuan Feng,[a,*] Chao Lu,[b] and P. K. A. Wai[b]

[a]*Institute of Photonics Technology, Jinan University, Guangzhou, 510632, China*
[b]*Photonics Research Centre, Department of Electronic and Information engineering, The Hong Kong Polytechnic University, Hong Kong SAR, China. 20036, USA*

Abstract

We theoretically study the transfer function of finite impulse response microwave photonic filter (FIR-MPF) system using multi-wavelength multi-longitudinal-mode fiber laser source when taking into consideration the influence of longitudinal-modes. The full response function with an additional term, namely the response from longitudinal-mode taps, is obtained. Furthermore we discussed the influence of the mode profile, bandwidth, profile termination by the threshold, and mode spacing of the longitudinal-modes to the performance of MPF. The response function of the additional term is fully discussed and the contribution is compared with the response of the carrier suppression factor for double sideband (DSB) modulation. The analysis provides a clear guideline for designing incoherent FIR-MPF systems.

Keywords: Microwave photonics filter, multi-wavelength fiber laser, multi-longitudinal-mode

1. Introduction

Microwave photonic filter (MPF) is a powerful technique to process microwave signals directly in the optical domain [1–10]. Compared with traditional electrical filter which is achieved by radio frequency (RF) circuits after a down-conversion operation, MPF offers the advantages of low loss, wide bandwidth, tunability, reconfigurability and immunity to electromagnetic interference (EMI) [1–5]. Based on the optical source used, MPFs can be divided into two categories: single-source based MPFs and multi-source based MPFs. The single-source MPF (SSMPF) requires that the coherent time of the light source is smaller than the minimum delay time of the system to ensure stable filter operation. Its performance is limited by phase induced intensity noise and the delay tuning can be difficult which limits the reconfigurability of the filter. The multi-source MPF (MSMPF) offers much promises, because the signals from different taps can be assumed to be always uncorrelated [6–8]. The optical source for a MSMPF could be a laser diode array [9, 10], spectrum slicing from a broadband source [11-13] or a Fabry–Pérot (F-P) laser [14]. However, laser diode array is expensive when the number of taps is large. Spectrum slicing will introduce large amplitude noises. The variation of mode power distribution in the F-P laser will limit its usefulness in filter implementation. Thus, finding a suitable optical source for MPF has been a challenge.

In our previous work, we demonstrated for the first time to our knowledge the use of multi-wavelength erbium-doped fiber laser (EDFL) as the optical source of a MPF and achieved the tunability of Q value [15]. Since then, many schemes of realizing MPFs based on multi-wavelength fiber laser source have been demonstrated [16–21]. But for a conventional multi-wavelength fiber laser, the cavity length is always more than 10 meters, which means the longitudinal-mode spacing is less than 20 MHz and plenty of longitudinal-modes exist in a single wavelength. However, conventional theories of incoherent finite impulse response (FIR) MPF consider the output of one wavelength to be single frequency and have not taken the influence of longitudinal-modes into account. Up till now, the influence of longitudinal-modes to the MPF has not discussed in detail.

In this paper, we theoretically study the response of FIR-MPF based on multi-wavelength laser source with multi-longitudinal-modes in each wavelength tap. The paper is organized as follows. In Section II, we deduce the

*Corresponding author at: Institute of Photonics Technology, Jinan University, Guangzhou, 510632, China

E-mail address:eexhfeng@gmail.com(Xinhuan Feng)

transfer function of the FIR-MPF with multi-wavelength multi-longitudinal-mode fiber laser source. In Section III, we discuss the transfer function and investigate the influence of the longitudinal-mode parameters. The comparison between the response of carrier suppression factor for double sideband (DSB) modulation and the response from longitudinal-mode taps are performed. Finally, the conclusions are summarized in Section IV.

2. Theoretical model and transfer function of MPF

Compared with spectrum slicing in which most of the power is filtered out, the multi-wavelength fiber laser works better in power efficiency for optical source. Moreover, the multi-wavelength fiber laser has a higher Signal to Noise Ratio and the wavelength spacing can be tuned [22]. Figure 1 shows the schematic of a dispersive fiber delay line based multi-wavelength incoherent FIR-MPF. The multi-wavelength optical carrier is intensity modulated by an intensity modulator driven by the input electrical signal. Each wavelength of the multi-wavelength optical carrier is referred as a wavelength tap. The modulated signal is injected into a dispersive fiber delay line which introduces different time delays for different wavelength taps. The optical signal is converted to electrical signal by a photo-detector. The electrical signals carried by different wavelength taps which show different time delays will interfere with each other to form the filtered output electrical signal.

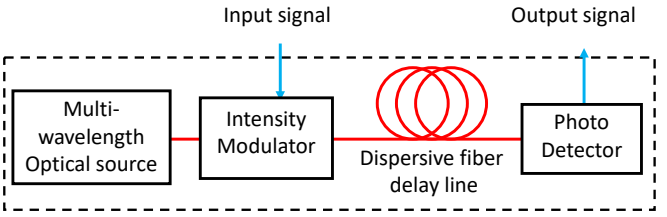

Fig. 1. Schematic of a multi-source incoherent microwave photonic filter.

With a fiber based cavity, the multi-wavelength laser source will have a cavity resonant frequency, which is also the longitudinal-mode spacing, that varies from kHz to MHz. Limited by the finesse of the comb filter adopted in the laser cavity to set the lasing wavelengths, the lasing channels of the multi-wavelength laser normally have linewidth much larger than the longitudinal-mode spacing. All the longitudinal-modes confined in the comb line profile and with positive net gain will eventually lase and contribute to the output signal. Thus in the FIR-MPF with multi-wavelength fiber laser source, there will be multi-longitudinal-modes in each wavelength taps.

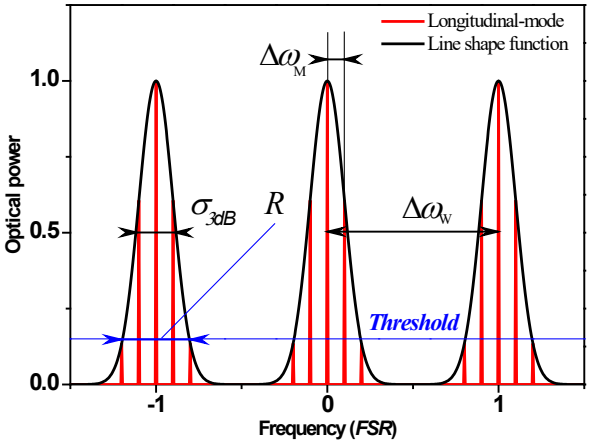

Fig. 2. The optical spectrum of a multi-wavelength multi-longitudinal-mode fiber laser.

In general, the amplitude of the output signal from such a multi-wavelength fiber laser can be defined as:

$$E_{MWL}(t) = \sum_{k=0}^{N-1}\left\{A_k \sum_{p=0}^{M-1} B_p \exp\left[-i\left(\omega_{kM+p}t + \phi_{kM+p}\right)\right]\right\}, \quad (1)$$

where $\omega_{kM+p} = \omega_0 + k\Delta\omega_W + p\Delta\omega_M$ and ϕ_{kM+p} are the angular frequency and initial phase of the p-th longitudinal-mode in the k-th wavelength tap, respectively. The angular frequency ω_0 is the first longitudinal-mode in the spectrum. The longitudinal-mode spacing $\Delta\omega_M$ is determined by the length of the laser cavity and the angular

frequency spacing $\Delta\omega_W$ is the wavelength taps as shown in Fig.2. The number of longitudinal-modes M in each wavelength tap is defined by $\Delta\omega_W/\Delta\omega_M$. The number of wavelength taps N in the whole spectrum is determined by the multi-wavelength laser output spectrum. The initial phases ϕ_{kM+m} are randomly chosen from 0 to 2π for different longitudinal-modes which means the lasing modes are not phase locked. For simplicity, the amplitude profiles of the longitudinal-modes in each wavelength taps are assumed to be the same, which is determined by the distribution of B_p. The amplitude of the modes in k-th wavelength tap can be adjusted as a group by the amplitude factor A_k.

In general, the phases of the lasing modes from the multi-wavelength laser source are independent which means ϕ_{kM+p} can be assumed to be randomized [7] and

$$\left\langle \exp\left[-i\left(\phi_a-\phi_b\right)\right]\right\rangle = 0, \quad a \neq b. \tag{2}$$

To investigate the transfer function of the FIR-MPF system, first we consider an RF signal with angular frequency Ω

$$V_M(t) = V_0 \cos\Omega t, \tag{3}$$

which will be applied to an intensity modulator to modulate the intensity of the multi-wavelength laser signal as

$$I_M(t) = I_{MWL}\left(1+m\cos\Omega t\right), \tag{4}$$

where $m \ll 1$ and $m \propto V_0$ is the modulation depth and I_{MWL} is the intensity of the incoherent signal defined in (1) as

$$I_{MWL} = \sum_{k=0}^{N-1}\sum_{p=0}^{M-1} A_k^{\,2} B_p^2. \tag{5}$$

It should be noted that the intensity modulation in (4) will generate double sidebands (DSB) in the optical spectrum. We only consider the DSB here because the single sideband (SSB) modulation can be considered as a linear combination of two DSB modulations with $\pi/2$ phase shift [7].

After the modulator, the electrical field amplitude of the optical signal will be

$$\begin{aligned} E_M(t) &= E_{MWL}(t)\times\sqrt{1+m\cos\Omega t} \\ &\approx E_{MWL}(t)\times\left(1+\frac{m}{2}\cos\Omega t\right). \end{aligned} \tag{6}$$

The modulated signal is injected into a section of dispersive fiber which will introduce time delays between the optical signals with different frequencies. While the spectral bandwidth is finite and only the second order dispersion coefficient β_2 is considered, the output signal from the dispersive fiber is [7]

$$\begin{aligned} E_{PD}(t) = &\left[1+\frac{m}{2}\exp\left(i\frac{1}{2}\beta_2 L\Omega^2\right)\cos\Omega(t-k\Delta\tau_W-p\Delta\tau_M)\right] \\ &\times\sum_{k=0}^{N-1}\sum_{p=0}^{M-1} A_k B_p \exp\left\{-i\left[\omega_{kM+p}\left(t-k\Delta\tau_W-p\Delta\tau_M\right)+\phi_{kM+p}\right]\right\}, \end{aligned} \tag{7}$$

where L is the length of the dispersive fiber. $\Delta\tau_M = \beta_2 L\Delta\omega_M$ and $\Delta\tau_W = \beta_2 L\Delta\omega_W = M\Delta\tau_M$ are the relative time delays between adjacent longitudinal-modes and adjacent wavelength taps respectively. Then the optical intensity detected by the photo detector is given by

$$I_{PD}(t) = \sum_{k=0}^{N-1}\sum_{p=0}^{M-1} A_k^2 B_p^2\left[1+m\cos\left(\frac{\beta_2 L\Omega^2}{2}\right)\cos\Omega\left(t-k\Delta\tau_W-p\Delta\tau_M\right)\right], \tag{8}$$

where the cross terms are all zero because of the incoherency of different lasing modes and the high order terms with m^2 are neglected. While Ω is an arbitrary selected frequency, the transfer function of the FIR-MPF is given by

$$\left|H(\Omega)\right| = \left|\frac{V_{PD}(\Omega)}{V_M(\Omega)}\right| = \left|\Gamma \frac{I_{PD}(\Omega)}{I_M(\Omega)}\right| = \left|\Gamma \cos\left(\frac{\beta_2 L\Omega^2}{2}\right)\sum_{k=0}^{N-1} A_k^2 e^{-i\Omega k\Delta\tau_W} \sum_{p=0}^{M-1} B_p^2 e^{-i\Omega p\Delta\tau_M}\right|, \tag{9}$$

where Γ is the conversion factor determined by the responsivity of the photodiode and the intensity modulator. The transfer function can be separated as

$$\left|H(\Omega)\right| = \left|\Gamma \cos\left(\frac{\beta_2 L\Omega^2}{2}\right) \times \sum_{k=0}^{N-1} A_k^2 e^{-i\Omega k\Delta\tau_W} \times \sum_{p=0}^{M-1} B_p^2 e^{-i\Omega p\Delta\tau_M}\right| = \left|\Gamma H_{DSB}(\Omega) \times H_W(\Omega) \times H_M(\Omega)\right|. \tag{10}$$

$H_{DSB}(\Omega)$ is the carrier suppression factor for DSB modulation. $H_W(\Omega)$ is the contribution to the transfer function of the wavelength taps. $H_M(\Omega)$ is the response from the longitudinal-modes in each wavelength tap which is the focus of this paper. It should be noted that when M = 1, only one longitudinal-mode survives in each wavelength tap, the response $H_M(\Omega)$ will be a constant B_0^2 which is 1 when a normalized profile is used to determine the distribution of B_p^2. Then the transfer function of the FIR-MPF is given by

$$\left|H'(\Omega)\right| = \left|\Gamma \cos\left(\frac{\beta_2 L\Omega^2}{2}\right)\sum_{k=0}^{N-1} A_k^2 e^{-i\Omega k\Delta\tau_W}\right| = \left|\Gamma H_{DSB}(\Omega) \times H_W(\Omega)\right|, \tag{11}$$

which agrees with reported results in [7].

From (10), the response for wavelength taps $H_W(\Omega)$ and longitudinal-modes $H_M(\Omega)$ are the discrete Fourier transform of the intensity profile A_k^2 and B_p^2.

3. Results and discussion

From (10), the multi-longitudinal-modes in each wavelength taps will introduce an extra factor $H_M(\Omega)$ to the transfer function when compared with the single longitudinal-mode wavelength taps FIR-MPF. To investigate the influence of $H_M(\Omega)$, we assume that all the wavelength taps have identical intensity, e.g. $A_k^2 = 1$. To clearly show the modulation detail of the response curve, the number of wavelength taps N is set to 7. In experiments, N depends on the bandwidth of the output spectrum and the FSR of the comb filter in the cavity used to set the lasing wavelength in the multi-wavelength laser source. The number of lasing wavelengths can vary from less than 10 to more than 50 [22]. With $A_k^2 = 1$, the response function $H_W(\Omega)$ will be the convolution of a *Sinc* function and a comb function with spacing of $FSR_W = 2\pi / \Delta\tau_W$. The *Sinc* function is the Fourier transform of the rectangular window function to set the wavelength taps number N. If other window functions or profiles are applied to the intensity distribution of the wavelength taps, then their Fourier transform will replace the *Sinc* function. The response curve of $H_W(\Omega)$ is shown as the black curve in Fig. 3. The carrier suppression factor for DSB $H_{DSB}(\Omega)$ will generate a nonlinear modulation with the increase of Ω. The modulation period will decrease with the increase of Ω as shown by the blue curve in Fig. 3.

Once the longitudinal-mode number M and the mode spacing $\Delta\omega_M$ are given, the response of the longitudinal-mode tap term $H_M(\Omega)$ will depend on the distribution profile of B_p^2. As mentioned in Section II, the response from the longitudinal-mode tap $H_M(\Omega)$ can be considered as the discrete Fourier transformation (DFT) of a series of discrete time domain signals B_p^2 with the sample interval being $\Delta\tau_M$:

$$\left|H_M(\Omega)\right| = \left|\sum_{p=0}^{M-1} B_p^2 \exp(-i\Omega p\Delta\tau_M)\right| = \left|\mathrm{DFT}(B_p^2)\right|. \tag{12}$$

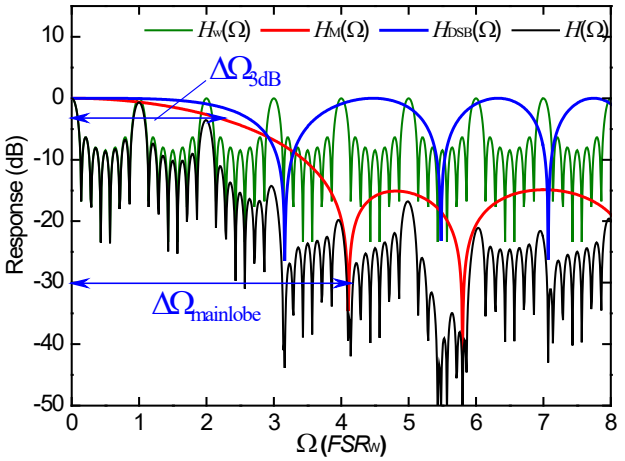

Fig. 3. The transfer function $H(\Omega)$ (green lines), carrier suppression factor of DSB modulation $H_{DSB}(\Omega)$ (blue lines), the response from wavelength taps $H_W(\Omega)$ (black) and the response from longitudinal-mode taps $H_M(\Omega)$ (red lines).

The distribution of B_p^2 can be defined by a profile function

$$B_p^2 = f\left(\omega_p\right). \tag{13}$$

In experiments, normally the lineshape of the lasing modes can be approximated by a Gaussian profile. Another notable feature of the laser lineshape is the termination of the profile by the noise floor. In the laser spectrum, only those longitudinal-modes with sufficient gain to compensate the loss can survive, which will confine the number of lasing modes in a finite frequency window for every wavelength taps. We used a rectangular window to model the termination of the lineshape profile. As the effect of noise is not considered in this paper, we will set the intensities of all other modes outside the rectangular windows to zero. Then the lineshape profile function can be modelled as

$$f(\omega) = \mathrm{RECT}\left(\frac{\omega-\omega_c}{R}\right)\cdot\exp\left[-\left(\frac{\omega-\omega_c}{\sigma_e}\right)^2\right], \tag{14}$$

where ω_c is the center frequency of the lineshape and R is the width of the rectangular window that confine the lasing modes as shown in Fig.2 and $\sigma_e = \sigma_{3dB}(4\ln 2)^{-1/2}$ is the width of the Gaussian profile. Use (13) and (14) in (12) and consider the discretization of B_p^2, we will get the transfer function as

$$\left|H_M(\Omega)\right| = \left|Sinc\left(\frac{\Omega\beta_2 LR}{2\pi}\right)\otimes\exp\left[-\left(\frac{\Omega\sigma_e\beta_2 L}{2}\right)^2\right] \otimes\sum_{n=-\infty}^{\infty}\delta(\Omega-n2\pi/\Delta\tau_M)\right|. \tag{15}$$

Fig. 4 shows the response curves of the *Sinc* function, Gaussian function and their convolution. The convolution curve shows similar oscillation structure to the *Sinc* function but the periods are not identical. The bandwidth of the main lobe from the convolution is larger than both of the *Sinc* and Gaussian functions. The intensities of the side lobes are simultaneously suppressed. The response from the longitudinal-mode tap $H_M(\Omega)$ and the total response $H(\Omega)$ are shown in Fig. 3 with colour red and black, respectively. It is interesting that both $H_{DSB}(\Omega)$ and $H_M(\Omega)$ show zero points which correspond to the deep notches on the response curve in log scale. Engineering the combination of such notches will enable us to suppress specific frequency response peaks to significantly increase the side mode suppression ratio. If the passing band located in low frequency region is desirable, the parameters of the longitudinal-mode structure can be engineered to enlarge the bandwidth of the main lobe of $H_M(\Omega)$ and minimize the suppression to the response in the desirable frequency.

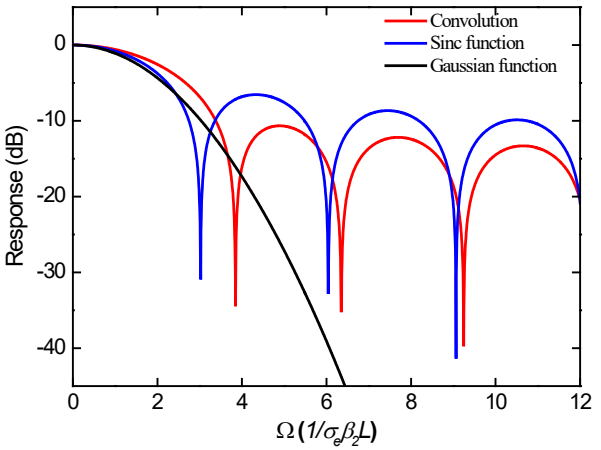

Fig. 4. The response from longitudinal-mode taps contributed by the *Sinc* function, Gaussian function and their convolution.

There are two parameters that can be used to characterize the response of $H_M(\Omega)$ as shown in Fig. 3. The 3dB bandwidth $(\Delta\Omega_{3\mathrm{dB}})$ will indicate the suppression to the response of low frequency region. The frequency where the first notch appears on $H_M(\Omega)$ indicates the maximum suppression to the response which can be defined as the bandwidth of the main lobe $(\Delta\Omega_{\text{main lobe}})$. Thus, to engineer the performances of the MPF, we should investigate the variation of $\Delta\Omega_{3\mathrm{dB}}$ and $\Delta\Omega_{\text{main lobe}}$ with the parameters of the longitudinal-mode structure.

We should notice that the response from the wavelength taps $H_W(\Omega)$ can also be analyzed with the DFT model. Only the details may be different.

3.1 The influence of lineshape parameters to σ_e.

In the response function (15), two independent parameters σ_e and R affect the lineshape. Since simultaneous variation of σ_e and R will not change the response curve shape but only change the scale, we can introduce a normalized window range $r = R/\sigma_e$, namely the ratio of the window width to the linewidth as an independent factor. Then the normalized $H_M(\Omega)$ can be describe by

$$\left|H_M(\Omega)\right| = \left|Sinc\left(\frac{r\Omega\sigma_e\beta_2 L}{2\pi}\right) \otimes \exp\left[-\left(\frac{\Omega\sigma_e\beta_2 L}{2}\right)^2\right]\right|. \tag{16}$$

The comb function will not appear in (16) if the spacing of the Dirac Delta (δ) functions is much larger than the bandwidth of the response function. Then we will only focus on the frequency region $0 < \Omega$ □ $FSR_M = 2\pi/\Delta\tau_M$. We will also introduce a normalized angular frequency $x = \Omega\sigma_e\beta_2 L$. Then the normalized frequency spectrum $H_M(\Omega)$ will be

$$\left|\bar{H}_M(x)\right| = \left|Sinc(r\cdot x/2\pi) \otimes \exp(-x^2/4)\right|. \tag{17}$$

Then there will be only one parameter r which will affect the shape of the response curve. From (17) we can obtain $\Delta\Omega_{\text{main lobe}} = x_0/(\sigma_e\beta_2\,\mathrm{L})$ and $\Delta\Omega_{3\mathrm{dB}} = x_{1/2}/(\sigma_e\beta_2\,\mathrm{L})$ by solving the normalized equations

$$\frac{d\left|\bar{H}_M(x)\right|}{dx} = 0, \frac{d^2\left|\bar{H}_M(x)\right|}{dx^2} > 0, \text{ and } \left|\bar{H}_M(x)\right| = 1/2, \tag{18}$$

respectively.

3.1.1. The scaling of response curve with linewidth σ_e.

The normalized response function (17) indicates that, if the value of r is given, the response function has only one variable x. If we vary the linewidth σ_e by a factor a as $\sigma_e' = a\sigma_e$, the response function shape will remain the

same if we scale the frequency as $\Omega' = \Omega/a$. Fig. 5 shows the scaling of the response function while σ_e varies from 1 to 3 with $r = 3$. The profiles of the response curves are similar but the scale on **Ω** is compressed.

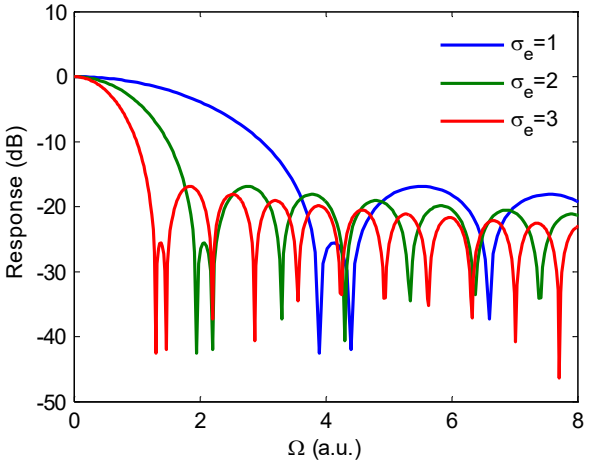

Fig. 5. The response curves $H_M(\Omega)$ with $\sigma_e = 1, 2, 3$.

3.1.2. The influence of the lineshape parameter ***r.***

The lineshape parameter r indicates the ratio of the bandwidth of the rectangular window R to the linewidth σ_e. It is obvious that r will change the shape of $\bar{H}_M(x)$ by scaling the *Sinc* function in (17). Fig. 6 shows the variation of the normalized response function when r varies from 1 to 5. When r = 1, which means the width of the rectangular window is equal to the linewidth σ_e, the contribution from the *Sinc* function will be dominant in the response curve which remains large even in high frequency region. When r increases, the *Sinc* function will be compressed on the x-axis. When r increases further, the Gaussian function becomes increasingly dominate since more and more of the Gaussian function is confined in the rectangular window. Thus the intensity of the side lobes will decrease. When $r > 7$, the main lobe will become insensitive to r and the side lobes are all suppressed.

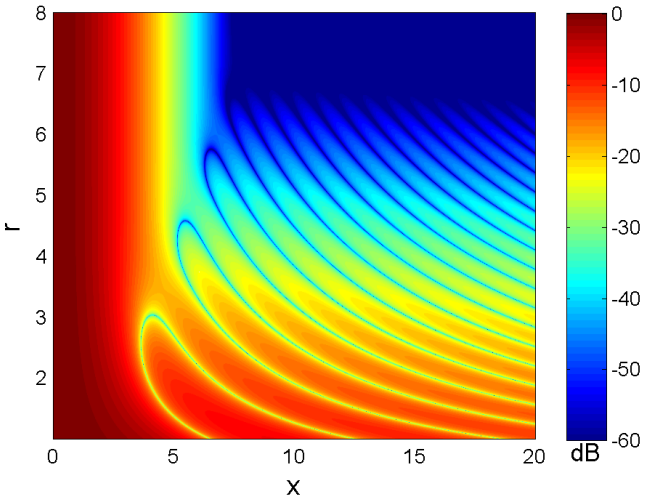

Fig. 6. Variation of the response function $\bar{H}_M(x)$ with increasing r.

Fig. 7(a) shows the variation of the main lobe bandwidth. The value of $x_{1/2}$ which indicates the 3-dB bandwidth decreases when r increases from 1 to 5 but remains almost unchanged for $r > 5$. When $r \to \infty$, the $Sinc(r \cdot x)$ function will become the Dirac Delta function $\delta(x)$ which will be transparent in convolution. Then the response

function will be just the Gaussian function and $x_{1/2}$ will approach the value $(4\ln 2)^{1/2}$ which is the 3-dB bandwidth of the Gaussian function. The bandwidth of the main lobe is determined by the first minimum point x_0 on the response curve which shows more complex dynamics as shown by the blue circles in Fig. 7(a). Fig. 7(b) shows the response function dynamics for $1.5 < r < 6$ and $3 < x < 7$. From Fig. 7(b), it is clear that when r increases, the $(2n-1)$-th and $2n$-th notch points, where n is a rational number, will attract each other and eventually merged. The $(2n-1)$-th and $2n$-th notch points will then disappear after the merging. The response function will show a valley near the merging point and the valley will quickly be flattened when r increases. Once the valley is flattened, the bandwidth of the main lobe will show a sudden increase because the first minimum point will abruptly switch to the $(2n+1)$-th notch point.

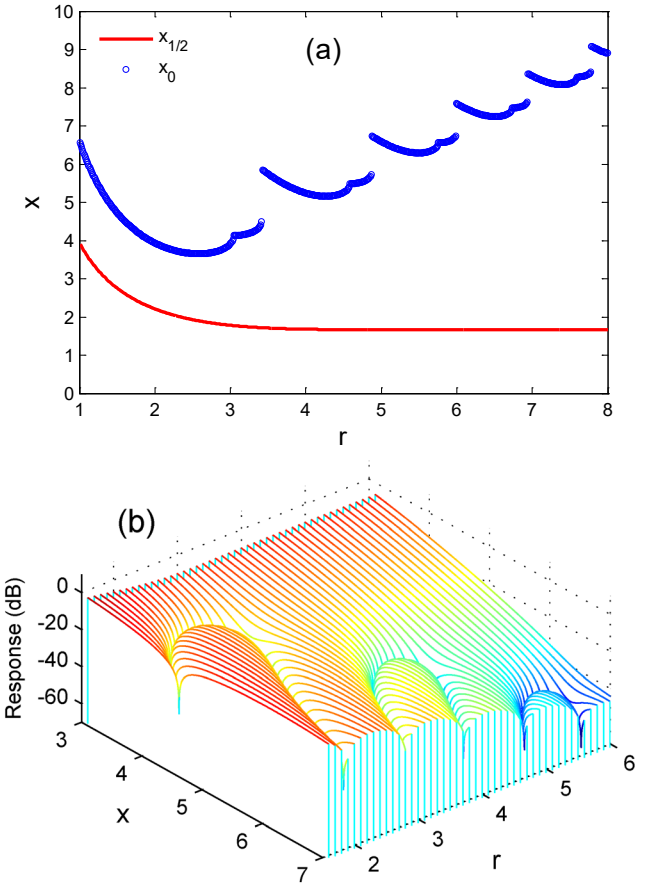

Fig. 7. (a) The variation of x_0 and $x_{1/2}$ with the increasing of r. (b) The response $\bar{H}_M(x)$ in the region $1.5 < r < 6$ and $3 < x < 7$.

3.2 The influence of the mode spacing $\Delta\omega_M$.

In the previous section, we have assumed that the spacing of the Dirac Delta functions FSR_M is much larger than the bandwidth of the response function so we only focus on the frequency region $0 < \Omega$ $FSR_M = 2\pi / \Delta\tau_M$. The spacing FSR_M is determined by the time delay $\Delta\tau_M$ which is proportional to the mode spacing $\Delta\omega_M$. To investigate the variation of the response function to the mode spacing, we introduce a relative ratio $h = \sigma_e / \Delta\omega_M$ which measures the longitudinal-mode number included in the bandwidth of the Gaussian profile function. Using the normalized frequency x, the normalized response function becomes

$$\left|\hat{H}_M(x)\right| = \left|Sinc(r\cdot x/2\pi)\otimes \exp[-x^2/4]\otimes \sum_{n=-\infty}^{\infty}\delta(x-2\pi nh)\right|$$
$$= \left|\bar{H}_M(x)\otimes \sum_{n=-\infty}^{\infty}\delta(x-2\pi nh)\right|. \quad (19)$$

Fig. 8 shows the variation of the response function for different values of h. Here we use $r = 6$ as a typical value. If $h \ll 1$ which means the longitudinal-mode spacing is much larger than the bandwidth of the wavelength taps, then there will be only one longitudinal-mode in each wavelength tap. The response contribution $\hat{H}_M(x)$ will become a constant as shown in Fig. 8(a). This means it will be transparent in the total response function of the FIR-MPF. When h increases, modulation will appear on the response function. The modulation depth as well as the modulation period $2\pi h$ will increase as shown in Fig. 8(b)-(c). When the separation of the peaks at $x = 2\pi nh$ increases, where $n \geq 0$ is a rational number, the overlapping of the peaks will decrease but the profiles of each individual peak determined by $\bar{H}_M(x)$ will remain unchanged. If h is sufficiently large, the peaks will be well separated and the overlapping will only slightly affect each other. The response will be totally suppressed in the regions outside the peaks at $x = 2\pi nh$.

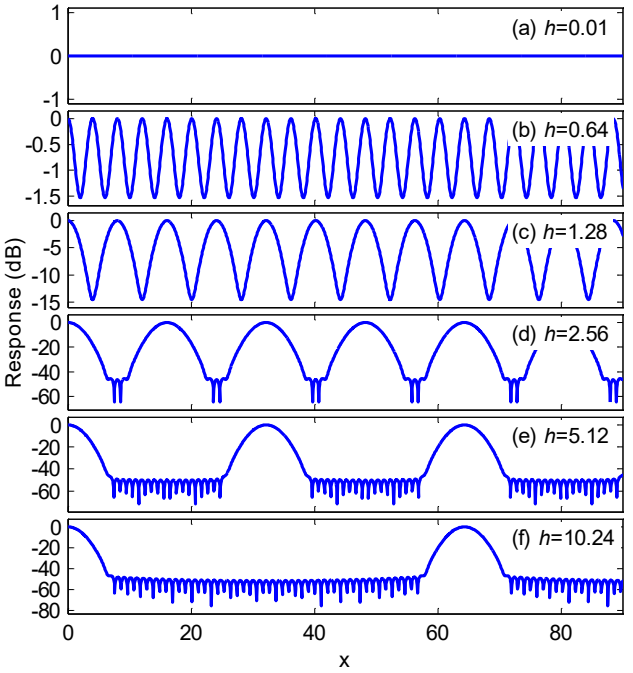

Fig. 8. The response $\hat{H}_M(x)$ when h varies from 0.01 to 10.24.

3.3 Comparison of $H_M(\Omega)$ and $H_{DSB}(\Omega)$.

From (10), three terms contribute to the response of the FIR-MPF. The contribution from the wavelength taps $H_W(\Omega)$ generates fast modulations on the response curve and the other two terms $H_M(\Omega)$ and $H_{DSB}(\Omega)$ generate envelopes on the response curve. Normally, $H_M(\Omega)$ and $H_{DSB}(\Omega)$ show similar modulations and comparable bandwidth in the main lobes. We compare them in detail to understand the two effect and their differences.

If we use the normalized angular frequency x, the carrier suppression factor $H_{DSB}(\Omega)$ will be written as

$$\left|H_{DSB}(x)\right| = \left|\cos\left(\frac{x^2}{2\chi}\right)\right|, \quad (20)$$

where $\chi = \sigma_e^2\beta_2 L$. Fig. 9(a) shows the response curves of $H_{DSB}(x)$ with $\chi = 1$ (red solid lines) and 2 (magenta solid lines), and $\bar{H}_M(x)$ with $r = 4$ (blue dashed lines). All the side lobes of $\bar{H}_M(x)$ drop to less than –20 dB and will be

even lower for larger r. The side lobes of $H_{DSB}(x)$ however remain at the peak value of 0 dB. The response of $H_{DSB}(x)$ is flatter and larger than that of $\bar{H}_M(x)$ in the low frequency region but it will drop faster than $\bar{H}_M(x)$ after the flat region. Even the side lobes of both curves of $H_{DSB}(x)$ appear earlier than the side lobes of $\bar{H}_M(x)$, the 3 dB loss points of the two curves are located on different sides of the 3 dB loss points of $\bar{H}_M(x)$. The curve of $H_{DSB}(x)$ with $\chi = 2$ has smaller main lobe bandwidth which is defined by the minimum point than that of $\bar{H}_M(x)$, but has larger 3 dB bandwidth than that of $\bar{H}_M(x)$. The 3 dB loss point of $H_{DSB}(x)$ can be solved directly by

$$\frac{x^2}{2\chi} = \frac{\pi}{3}. \tag{21}$$

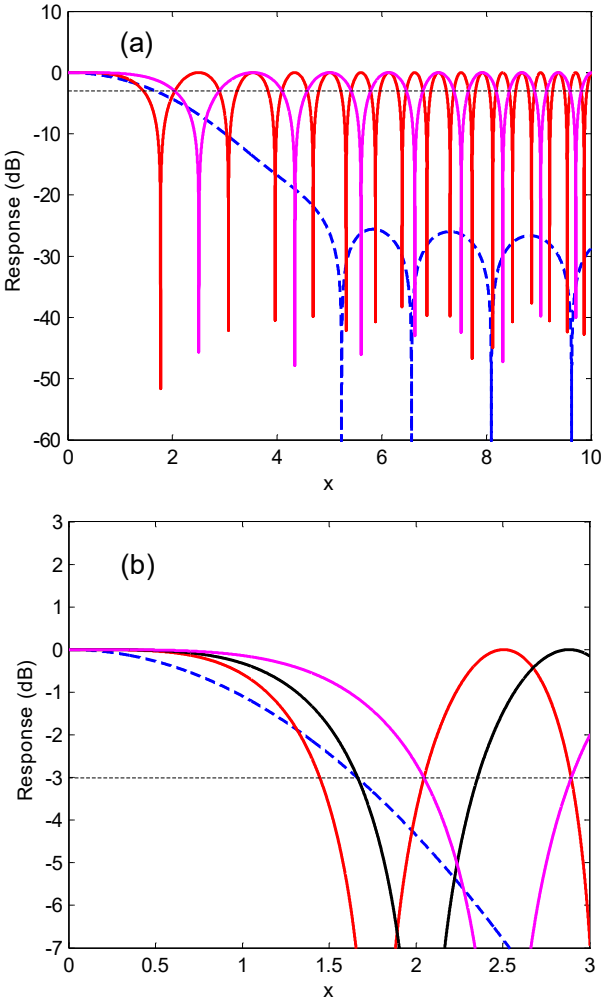

Fig. 9. (a) The carrier suppression factor for DSB modulation $H_{DSB}(x)$ with $\chi = 1$(red solid line), $\chi = 2$(magenta solid lines), and $\bar{H}_M(x)$ with $r = 4$(blue dashed lines). (b) The carrier suppression factor for DSB modulation $H_{DSB}(x)$ with $\chi = 1$(red solid lines), $\chi = 6\ln 2/\pi$ (black solid lines), $\chi = 2$(magenta solid lines), and $\bar{H}_M(x)$ with $r \to \infty$ (blue dashed lines). The black dashed horizontal lines indicate the −3 dB level.

As for $\bar{H}_M(x)$, the 3 dB loss point can be found analytically when $r \to \infty$. The solution is $x = 2(\ln 2)^{1/2}$. So $\bar{H}_M(x)$ and $H_{DSB}(x)$ will have the same 3 dB bandwidth when $\chi = 6\ln 2/\pi$. Fig. 9(b) show the response curve of $\bar{H}_M(x)$ when $r \to \infty$ (blue dashed lines), and the curves of $H_{DSB}(x)$ with $\chi = 1$ (red solid lines), $\chi = 6\ln 2/\pi$ (black solid

lines) and $\chi = 2$ (magenta solid lines) . It shows that the blue dashed curve cross the black solid curve at the point with response –3 dB.

In the realization of MPF, SSB can be adopted to eliminate the response penalty induced by the term $H_{DSB}(x)$. In the MPF system with SSB, the longitudinal-mode tap term $\bar{H}_M(x)$ will dominate the penalty on the performance of the MPF system.

3.4 Engineering the FIR-MPF response with $H_M(\Omega)$.

By introducing the normalized frequency x and the relative rectangular window width r, we know the longitudinal-mode tapping will add extra modulation on the response function of the FIR-MPF. The longitudinal-mode tapping provides another freedom to manage the response function of the FIR-MPF. For example, by engineering the parameters of the FIR-MPF, we can realize desirable filter response function with large side mode suppression ratio. As an illustration, we assume that the multi-wavelength laser generates 30 wavelength taps with a frequency spacing $\Delta\omega_W$ = 100 GHz and the longitudinal-mode spacing $\Delta\omega_M$ = 1 MHz. If we want to realize a FIR-MPF response function with FSR = 20 GHz, which corresponding to $\Delta\tau_W$ = 50 ps, the dispersion fiber length product $\beta_2 L$ should be selected as 500 ps^2. Here we focus on the combination of the response from the wavelength taps and longitudinal taps. Fig. 10 shows the response curves of the wavelength taps (red lines), longitudinal taps(black) and the combined response (blue lines). The 3-dB width of the longitudinal-mode profile $\sigma_{3\text{dB}}$ is 11 GHz and the threshold window ratio r is chosen as 4.

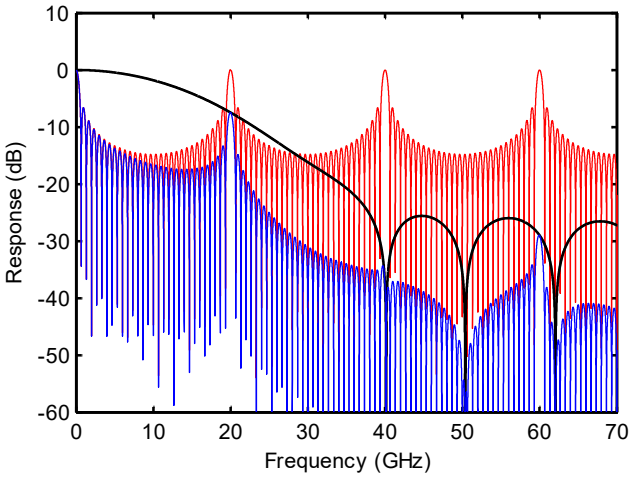

Fig. 10. The response curves of engineered wavelength taps (red lines), longitudinal-mode taps (black lines) and the combination of the two (blue lines)

As shown in Fig. 10, the 2-nd side lobe of the response curve is significantly suppressed. If we adopt a phase modulation in the system to suppress the peak at zero frequency [21], then we can realize a single bandpass FIR-MPF. Actually, the carrier suppression factor for DSB modulation $H_{DSB}(\Omega)$ will also show quasi-periodic modulation in the response which can be adopted to engineer the response. But the response $H_{DSB}(\Omega)$ depends only on the fiber parameters including the dispersion and the fiber length which cannot be changed after the fabrication of the FIR-MPF system. The longitudinal-mode profile however can be engineered through engineering the laser source which is more flexible.

4. Conclusion

We theoretically study the transfer function of multi-wavelength FIR-MPF when considering the effect of laser longitudinal-modes. The full response function including the contribution from the longitudinal-mode taps is obtained. We discussed the effects of the mode profile, bandwidth, termination by the threshold, and mode spacing of the longitudinal-modes to the performance of MPF. We studied the response function in detail and compared the contribution of the response of the carrier suppression factor for double sideband modulation.

The response function of the FIR-MPF with multi-longitudinal-modes is the convolution of three terms: the carrier suppression factor $H_{DSB}(\Omega)$, the contribution from wavelength taps $H_W(\Omega)$, and the contribution from the longitudinal-modes $H_M(\Omega)$. The contribution of $H_M(\Omega)$ is determined by the mode profile of each wavelength tap, the dispersion of the fiber, and the fiber length. If the fiber used in the cavity is chosen, the mode profile will determine $H_M(\Omega)$. The bandwidth of the mode profile will affect the bandwidth of the main lobe. When the termination to the gain profile is considered, the final mode profile shape will affect the amplitude of the side lobes and the bandwidth of the main lobe. If the mode spacing is very large such that only a few modes survive in a wavelength tap, the overlapping of the adjacent orders on the response curve $H_M(\Omega)$ will maintain the amplitude on a high level in the whole range. A major difference between the response $H_M(\Omega)$ and $H_{DSB}(\Omega)$ is that the side lobes of $H_M(\Omega)$ will drop to a low amplitude level but the side lobes of $H_{DSB}(\Omega)$ will not drop. In some parameter regime, the bandwidth of $H_M(\Omega)$ will be comparable to $H_{DSB}(\Omega)$.

The analysis provides a clear guideline for designing incoherent FIR-MPF systems.

Acknowledgements

This work was supported in part by the Natural Science Foundation of Guangdong Province of China (No S2012010008850), and the Fundamental Research Funds for the Central Universities in China (21612201).

References

[1] J. Capmany, B. Ortega and D. Pastor, A tutorial on microwave photonic filters, J. Lightwave. Technol. 24(1) (2006) 201–229.
[2] R. A. Minasian, Photonic signal processing of microwave signals, IEEE Trans. Microw. Theory Tech. 54(2) (2006) 832–846.
[3] Jianping Yao, Microwave photonics, J. Lightwave. Technol. 27(3) (2009) 314–335.
[4] Fei Zeng and Jianping Yao, All-optical bandpass microwave filter based on an electro-optic phase modulator, Opt. Express 12(16) (2004) 3814-3819.
[5] J. Marti, F. Ramos, and R. I. Laming, Photonic microwave filter employing multimode optical sources and wideband chirped gratings, Electron. Lett. 34(18) (1998) 1760–1761.
[6] D. B. Hunter and R. A. Minasian, Tunable transversal filter based on chirped gratings, Electron. Lett. 31(25) (1995) 2205–2207.
[7] J. Capmany, D. Pastor, and B. Ortega, New and flexible fiber-optic delay-line filters using chirped fiber Bragg gratings and laser arrays, IEEE Trans. Microw. Theory Tech. 47(7) (1999) 1321–1326.
[8] G. Yu, W. Zhang, and J. A. R. Williams, High-performance microwave transversal filter using fiber Bragg grating arrays, IEEE Photon. Technol. Lett. 12(9) (2000) 1183–1185.
[9] V. Polo, B. Vidal, J. L. Corral, and J. Marti, Novel tunable photonic microwave filter based on laser arrays and N/spl times/N AWG-based delay lines, IEEE Photon. Technol. Lett. 15(4) (2003) 584–586.
[10] J. Mora, S. Sales, M. D. Manzanedo, R. García-Olcina, J. Capmany, B. Ortega, and D. Pastor, Continuous tuning of photonic transversal filter based on the modification of tapped weights, IEEE Photon. Technol. Lett. 18(15) (2006) 1594–1596.
[11] B. Vidal, M.A. Piqueras and J. Marti, Photonic microwave filter based on spectrum slicing with reconfiguration capability, Electron. Lett. 41(23) (2005) 1286–1287.
[12] J. Mora, B. Ortega, J. Capmany, J. L. Cruz, M. V. Andres, D. Pastor, and S. Sales, Automatic tunable and reconfigurable fiber-optic microwave filters based on a broadband optical source sliced by uniform fiber Bragg gratings, Opt. Express 10(22) (2002) 1291–1298.
[13] Xiaoke Yi and R. A. Minasian, Dispersion induced RF distortion of spectrum-sliced microwave-photonic filters, IEEE Trans. Microw. Theory Tech. 54(2) (2006) 880–886.
[14] D. Pastor, J. Capmany, S. Sales, P. Munoz, and B. Ortega, Reconfigurable fiber-optic-based RF filters using current injection in multimode lasers, IEEE Photon. Technol. Lett. 13(11) (2001) 1224–1226.
[15] Xinhuan Feng; C. Lu; H.Y. Tam; P.K.A. Wai , Reconfigurable microwave photonic filter using multiwavelength Erbium-Doped Fiber Laser, IEEE Photon. Technol. Lett. 19(17) (2007) 1334-1336.
[16] Ehsan Hamidi, Daniel E. Leaird and Andrew M. Weiner, Tunable programmable microwave photonic filters based on an Optical Frequency Comb, IEEE Trans. Microw. Theory Tech. 58(11) (2010) 3269-3278.
[17] Haiyan Ou, Hongyan Fu a, Daru Chen and Sailing He , A tunable and reconfigurable microwave photonic filter based on a Raman fiber laser, Opt. Comm. 278(1) (2007) 48-51.
[18] Junqiang Zhou, Songnian Fu, Feng Luan, Jia Haur Wong , S. Aditya, P. P. Shum and K. E. K. Lee, Tunable multi-tap bandpass microwave photonic filter using a windowed Fabry-Perot filter-based multi-wavelength tunable laser, J. Lightwave. Technol. 29(22) (2011) 3381–3386.
[19] Xiaoke Yi, T.X.H. Huang, Liwei Li, R.A. Minasian, Overcoming Tap-Delay-Variation induced distortion in microwave photonic filters, IEEE Photon. Technol. Lett. 24(8) (2012) 691-693.

[20] Javier Abreu-Afonso, Antonio Díez, Jose Luis Cruz and Miguel V. Andrés, Continuously Tunable Microwave Photonic Filter Using a Multiwavelength Fiber Laser, IEEE Photon. Technol. Lett. 24(23) (2012) 2129-2131.
[21] Yuan Cao, Haiyan Shang, Xinhuan Feng, Zhaohui Li, Bai-ou Guan, Investigation of microwave photonic filter based on multiwavelength phase modulation and spectral shaping, Opt. Eng. 51(11) (2012) 115002.
[22] Moon, D. S., Kim, B. H., Lin, A., Sun, G., Han, W. T., Han, Y. G., Chung, Y. , Tunable multi-wavelength SOA fiber laser based on a Sagnac loop mirror using an elliptical core side-hole fiber, Opt. Express. 15(13) (2007) 8371-8376.
[23] X. H. Feng, H. Y. Tam, H. L. Liu, and P. K. A. Wai. Multiwavelength erbium-doped fiber laser employing a nonlinear optical loop mirror, Opt. Comm. 268(2) (2006) 278–281.